Oscillatory clusters in a model of the photosensitive Belousov-Zhabotinsky reaction system with global feedback

Lingfa Yang, Milos Dolnik,* Anatol M. Zhabotinsky, and Irving R. Epstein
Department of Chemistry and Center for Complex Systems, MS 015, Brandeis University, Waltham, Massachusetts 02454-9110
(Received 22 May 2000)

Oscillatory cluster patterns are studied numerically in a reaction-diffusion model of the photosensitive Belousov-Zhabotinsky reaction supplemented with a global negative feedback. In one- and two-dimensional systems, families of cluster patterns arise for intermediate values of the feedback strength. These patterns consist of spatial domains of phase-shifted oscillations. The phase of the oscillations is nearly constant for all points within a domain. Two-phase clusters display antiphase oscillations; three-phase clusters contain three sets of domains with a phase shift equal to one-third of the period of the local oscillation. Border (nodal) lines between domains for two-phase clusters become stationary after a transient period, while borders drift in the case of three-phase clusters. We study the evolving border movement of the clusters, which, in most cases, leads to *phase balance*, i.e., equal areas of the different phase domains. *Border curling* of three-phase clusters results in formation of spiral clusters—a combination of a fast oscillating cluster with a slow spiraling movement of the domain border. At higher feedback coefficient, irregular cluster patterns arise, consisting of domains that change their shape and position in an irregular manner. Localized irregular and regular clusters arise for parameters close to the boundary between the oscillatory region and the reduced steady state region of the phase space.

PACS number(s): 47.54.+r, 82.20.Mj, 82.40.Bj

I. INTRODUCTION

The Belousov-Zhabotinsky (BZ) reaction has been widely used as a prototype system for the study of chemical oscillations and pattern formation for over 30 years. The BZ reaction-diffusion system has been utilized primarily to understand the dynamics of patterns consisting of traveling waves, including target patterns and spiral waves [1–3]. The nontraveling types of patterns found in other chemical oscillating systems have not been observed in the autonomous, homogeneous BZ reaction. Examples of nontraveling patterns include Turing structures and standing oscillatory patterns: waves and clusters. Clusters consist of sets of domains in which nearly all of the elements in a domain oscillate with the same amplitude and phase [4–8]. They resemble standing waves, but possess no intrinsic wavelength.

The requirements for obtaining Turing structures do not favor the BZ system, owing to an unsuitable ratio of diffusion coefficients for the autocatalytic and inhibitory species. Standing oscillatory patterns do not naturally arise in the BZ reaction. Until recently, standing waves and clusters have been observed only in heterogeneous systems, e.g., during electrochemical dissolution of nickel [9], oxidation of CO on a Pt catalyst [10], hydrogen oxidation on a nickel ring [11], and methylamine oxidation on Rh [12]. Global feedback interactions play important roles during these heterogeneous processes, and they are responsible for the occurrence of standing patterns. In contrast, homogeneous reactions, unless they are specifically designed, do not possess these global interactions and therefore they do not commonly display standing patterns. Nevertheless, studies with a simple model of an autonomous homogeneous chemical reaction demonstrate that standing waves may arise in homogeneous systems via the short-wave instability [13–15].

The photosensitive $Ru(bpy)_3$-catalyzed BZ reaction provides an effective way to control oscillations by light illumination. Standing waves in the photosensitive BZ system were first reported in a nonautonomous system with external periodic forcing [16]. Recently, experimental observation of a family of oscillatory clusters has been reported in the BZ reaction-diffusion system with photochemical global feedback (GF) [17]. The experiment described in Ref. [17] employs the transmission of analyzing light through the working area of a gel layer to measure the average concentration of $Ru(bpy)_3^{3+}$. This quantity is used to determine the intensity of the actinic light, which creates a photochemical global feedback control.

Here, we study an autonomous model of the photosensitive $Ru(bpy)_3$-catalyzed BZ reaction with a global feedback, which corresponds to the experiment described in Ref. [17]. In our study we assume a proportional dependence between the actinic light intensity and the difference between the average concentration of $Ru(bpy)_3^{3+}$ and a target concentration. We call this proportionality constant the feedback coefficient, and we study pattern formation as a function of this parameter. Our simulations in one- and two-dimensional systems exhibit a plethora of patterns, including two-phase and three-phase clusters and other, more complex clusters.

II. MODEL AND METHOD OF SIMULATION

We study pattern formation in a quantitative model of the BZ reaction with a realistic global feedback coupling. In the photosensitive $Ru(bpy)_3$-catalyzed BZ reaction, illumination results in production of Br^- ions via reduction of bromomalonic acid by the excited $Ru(bpy)_3^{2+}$ ion [18]. The model,

*Author to whom correspondence should be addressed.

based on a simplified, two-variable version of the BZ reaction model [19,20], is

$$\frac{\partial X}{\partial t}=\frac{-k_2X+k_3A}{k_2X+k_3A}\left[qk_7k_8\frac{BZ}{k_8+k_{-7}h_0(C-Z)}+k_9B+\gamma(Z_{av}-Z_t)\right]-2k_4X^2+k_5h_0AX-k_{-5}U^2+D_x\frac{\partial^2X}{\partial r^2}, \tag{1}$$

$$\frac{dZ}{dt}=k_6U(C-Z)-k_{-6}XZ-\frac{k_7k_8BZ}{k_8+k_{-7}h_0(C-Z)}+D_z\frac{\partial^2Z}{\partial r^2}, \tag{2}$$

where

$$U=\frac{-k_6(C-Z)+\sqrt{[k_6(C-Z)]^2+8k_{-5}(2k_5h_0AX+k_{-6}XZ)}}{4k_{-5}} \tag{3}$$

Here $X=[HBrO_2]$, $Z=[Ru(bpy)_3{}^{3+}]$, $U=[HBrO_2{}^+]$, $A=[HBrO_3]=h_0A_0/(h_0+0.2)$, $A_0=[NaBrO_3]$, B is the concentration of malonic acid, C is the total concentration of catalyst $[Ru(bpy)_3{}^{3+}]+[Ru(bpy)_3{}^{2+}]$, h_0 is the Hammett acidity function, and D_x, D_z are the diffusion coefficients. Z_{av} is the instantaneous spatial average of Z and Z_t is the target value of the oxidized form of the catalyst, which is set to correspond to Z_{ss}, the unstable steady state concentration. The parameter γ is the feedback coefficient, which depends on the maximum actinic light intensity and on the quantum yield of the photochemical reaction [17].

The GF in Eq. (1) represents an indirect (off-diagonal) feedback, rather than the more commonly encountered direct (diagonal) feedback [11]. This choice corresponds to the real experimental situation, where one observes the changes in the concentration of the oxidized and reduced forms of the $Ru(bpy)_3$ complex and thus measures the Z variable, while the actinic light directly influences $[HBrO_2]$, the X variable. The parameters and constants used in our simulations are shown in Table I; the feedback coefficient γ is the variable parameter. Simulations of the one- and two-dimensional reaction-diffusion system are performed using a finite-difference approximation to Eq. (1). The corresponding system of ordinary integro-differential equations is solved using the Euler method with adjustable time step. The maximum step used in the simulations is 2×10^{-2} s. The number of grid points varies with the length of the system. Unless stated otherwise, the size of the one-dimensional system is 10 mm and we use 30 grid points per millimeter; the size of the two-dimensional system is 10×10 mm^2 with a resolution of 20 grid points per millimeter. Neumann (zero-flux) boundary conditions are employed in most of the simulations. We use spatially uniform and random initial conditions, stationary patterns from previous runs, and some specially designed initial conditions.

TABLE I. Rate constants and parameters of Eq. (1).

k_2	$(M^{-2}\ s^{-1})$	2.0×10^6	$A_0(M)$	0.5
k_3	$(M^{-2}\ s^{-1})$	2.0	$B(M)$	0.27
k_4	$(M^{-1}\ s^{-1})$	3.0×10^3	$C(M)$	2.0×10^{-3}
k_5	$(M^{-2}\ s^{-1})$	3.3×10	$h_0(M)$	0.55
k_{-5}	$(M^{-1}\ s^{-1})$	4.2×10^6	q	0.7
k_6	$(M^{-1}\ s^{-1})$	4.0×10^6	$D_x(cm^2\ s^{-1})$	1.5×10^{-5}
k_{-6}	$(M^{-1}\ s^{-1})$	3.0×10^2	$D_z(cm^2\ s^{-1})$	2.0×10^{-6}
k_7	$(M^{-1}\ s^{-1})$	9.2×10^{-1}		
k_8/k_{-7}		2.5×10^{-4}		
k_9	(s^{-1})	3.0×10^{-6}		

III. RESULTS

A. Local dynamics

We first analyze the dynamics of model (1) without diffusion terms, which corresponds to a well-mixed system. Figure 1 shows a bifurcation diagram in the B-h_0 parametric space for the feedback-free system ($\gamma=0$). Hopf bifurcation lines separate the region of sustained oscillations from regions of reduced and oxidized steady states. In the following simulations we choose parameters $B=0.27M$ and $h_0=0.55M$ from the oscillatory region (point P in Fig. 1). The oscillatory behavior at this point is displayed in Fig. 2(a), and the effect of the feedback is shown in Fig. 2(b). The amplitude and frequency of oscillation remain almost unchanged for $0<\gamma<0.8\ s^{-1}$, but at larger values of the feedback coefficient the limit cycle is strongly affected. The amplitude and period of oscillations decrease as the feedback coefficient is increased. If the target value Z_t is set to the steady state value Z_{ss}, the feedback does not affect the stability of the steady state.

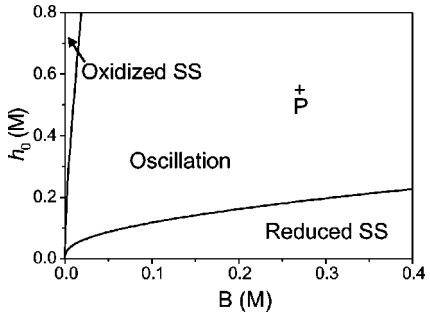

FIG. 1. Bifurcation diagram of the well-stirred ruthenium-catalyzed BZ reaction without feedback. The Hopf bifurcation lines divide the parametric plane B-h_0 into domains of sustained oscillation, steady state with high concentration of $Ru(bpy)_3{}^{2+}$ (reduced SS), and steady state with high concentration of $Ru(bpy)_3{}^{3+}$ (oxidized SS). Unless otherwise stated, simulations are performed with parameters corresponding to point P. Other parameters used in simulations are shown in Table I.

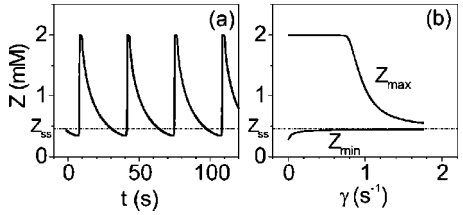

FIG. 2. Oscillations of $[Ru(bpy)_3^{3+}]$ in the well-stirred system. (a) Oscillations in system without feedback. (b) Effect of feedback coefficient γ on maximum and minimum concentrations of $Ru(bpy)_3^{3+}$ during oscillation. Z_{ss} is unstable steady state concentration of $Ru(bpy)_3^{3+}$.

B. Bulk oscillations and traveling waves at weak global feedback

We study pattern formation in one- and two-dimensional extended systems. Figure 3 displays a diagram of the basic types of pattern observed: bulk oscillations (BO's) and traveling waves (TW's) without feedback or at weak feedback, two-phase (C2) and three-phase (C3) clusters at intermediate intensity of GF, and irregular clusters (IC's) at relatively high levels of feedback. Eventually, IC's are suppressed at very high feedback coefficient and small-amplitude bulk oscillations (SBO's) emerge.

A simulation starting from a traveling wave pattern in a one-dimensional (1D) system evolves to a uniform, periodically oscillating pattern in a feedback-free system. In a 2D system some spiral waves are stable without feedback. Both BO's and TW's are stable when the feedback is weak. The ranges of γ in which bulk oscillations and traveling waves are stable overlap, which indicates that the pattern formation is dependent on the initial conditions. Spatially uniform initial conditions always lead to BO's when $\gamma < 0.8\ s^{-1}$. We obtain spiral waves, target patterns, and alternating traveling waves in our 2D simulations for $\gamma < 0.6\ s^{-1}$ from nonuniform initial conditions.

C. Oscillatory cluster patterns

1. Two-phase clusters

When the feedback coefficient exceeds $0.6\ s^{-1}$, in the case of random or traveling wave initial conditions, or $0.8\ s^{-1}$ in the case of spatially uniform initial conditions, two-phase clusters emerge. These clusters have fixed spatial domains and oscillate periodically in time; they resemble standing waves, but their spatial domains are determined by the initial conditions, and they possess no intrinsic wavelength. Figure 4(a) shows an example of two-phase clusters arising from a spiral wave. The rotational movement of the spiral stops after increase of the feedback coefficient, while the spiral shape is preserved. The clusters have two distinct phases half a period apart, which leads to antiphase periodic oscillation of domains with different phases [see Figs. 4(b) and 4(c)]. Domains with different phases are separated by nodal lines, which, after a transient period, become stationary and do not change their position with time. The emergence of stationary C2 clusters in this system usually proceeds via very long transients. The tiny changes in the nodal lines hardly visible in Fig. 4(b) are indications of these long-lived transients.

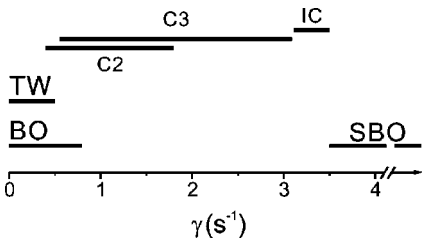

FIG. 3. Parametric diagram of 1D system with zero-flux boundary conditions. BO, bulk oscillations; SBO, small-amplitude BO; TW, traveling waves; C2, two-phase clusters; C3, three-phase clusters; IC, irregular clusters.

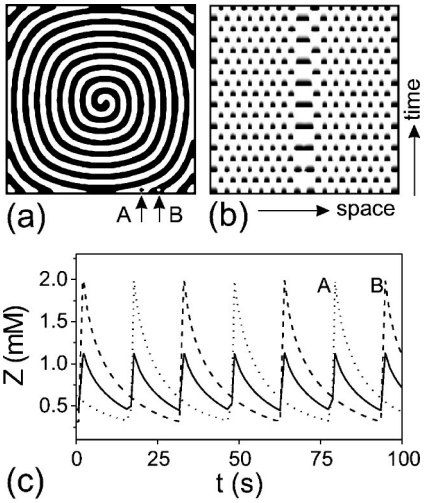

FIG. 4. Two-phase cluster arising from spiral wave, $\gamma = 1\ s^{-1}$. (a) Snapshot of a 2D pattern at time 400 s. (b) Spatiotemporal behavior along a vertical line at midpoint of horizontal axis. Time shown corresponds to 260 s. (c) Local oscillations at points *A* (dotted line) and *B* (dashed line) together with oscillations of average concentration Z_{av} (solid line). Gray levels represent $[Ru(bpy)_3^{3+}]$, with black corresponding to the maximum and white to minimum concentration. Size of system is $10 \times 10\ mm^2$.

When cluster patterns arise from random initial conditions, they always contain in the early stages many small spots of different shapes with sharp corners and large curvatures, as shown in Fig. 5(a). In the later stages of the evolution, the smallest spots disappear and the nodal lines separating domains become smoother due to a curvature effect [Figs. 5(b) and 5(c)]. Figure 5(d) shows this coarsening process in a space-time plot. Although the oscillatory cluster patterns do not possess a characteristic wavelength, these patterns require a minimum wavelength in order to be stationary. Therefore, to obtain stationary cluster patterns from random initial conditions, one needs to run the integration for a long time. As Fig. 5(d) indicates, the coarsening process takes close to a hundred periods of oscillation.

Another property of C2 clusters is *phase balance*, equality of areas occupied by the two domain types. If the initial conditions do not satisfy this equal area property, then the nodal lines slowly drift during the transient period until phase balance is attained. In a 1D system the lengths of the domains of the minority phase increase monotonically. Figure 6 shows a 1D simulation with initial conditions such that

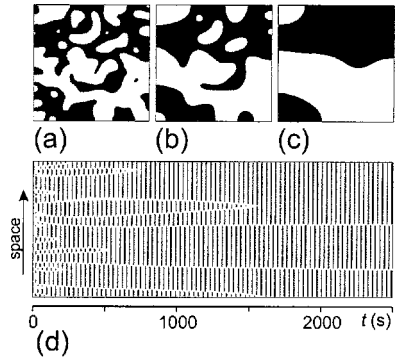

FIG. 5. Two-phase cluster pattern obtained from random initial conditions, $\gamma = 1\ s^{-1}$. Sequence of the oscillatory cluster pattern taken at (a) $t = 250$ s (b) $t = 750$ s, and (c) $t = 4300$ s. (d) Pattern evolution along the bottom left–top right diagonal. Size of system is $10 \times 10\ mm^2$.

the ratio of lengths of the two phases is $L1:L2 = 1:3$. One can see that after about 100 periods of oscillation the lengths of the two domain types are almost equal. In 2D systems, the balance between domains is also reached, but the transient processes are more complex because of the curvature effect.

2. Three-Phase Clusters

When the feedback coefficient exceeds $\gamma = 1.8\ s^{-1}$, the C2's become unstable and three-phase patterns arise. The phases of C3 clusters are shifted by one-third of the period of the local oscillations (T). Figure 7 shows an example of a C3 pattern obtained from random initial conditions. The domains of the three clusters with low, medium, and high levels of $[Ru(bpy)_3{}^{3+}]$ are displayed as white, gray, and black, respectively. After one-third of the period T, the white domains become black, black domains become gray, and gray turns to white. After a full period, the levels of $[Ru(bpy)_3{}^{3+}]$ repeat. Figure 7(d) shows the oscillatory behavior of each phase together with the average concentration Z_{av}. The borders between adjacent domains contain continuous levels of $Ru(bpy)_3{}^{3+}$. When a gray (intermediate $[Ru(bpy)_3{}^{3+}]$) domain is adjacent to a black (high $[Ru(bpy)_3{}^{3+}]$) domain, the border also contains low

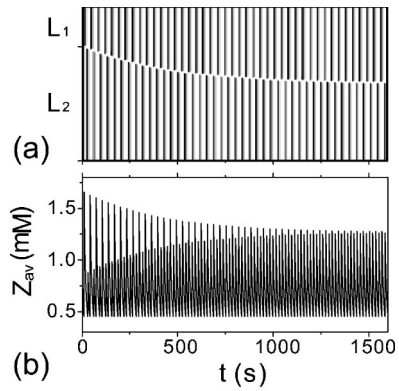

FIG. 6. Evolution of phase balance between domains of two-phase standing cluster in 1D system with initial ratio of phase domain sizes 1:3; $\gamma = 1\ s^{-1}$. (a) Spatiotemporal behavior. (b) Oscillations of average concentration of $Ru(bpy)_3{}^{3+}$. Length of system is 10 mm.

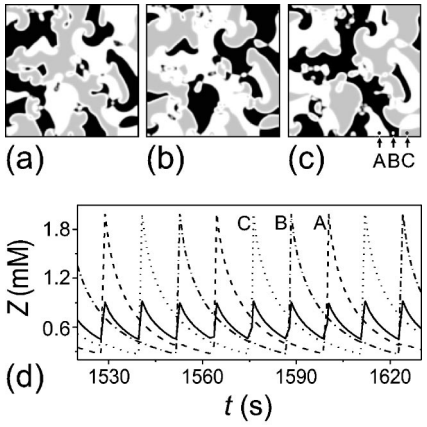

FIG. 7. Three-phase clusters, $\gamma = 2.5\ s^{-1}$. Snapshots (a), (b), and (c) are taken at time intervals 11.88 s apart, which corresponds to one-third of local oscillation period. (d) Local oscillations at points *A*, *B*, *C* of frame (c) together with oscillations of average concentration Z_{av} (solid line). Size of the system is $10 \times 10\ mm^2$.

$[Ru(bpy)_3{}^{3+}]$, which is displayed as white; one can always see a narrow white line between gray and black domains in Figs. 7(a), (b), and (c). The time sequence shown in Fig. 7(d) displays periodic oscillations at three points of space. However, individual points undergo periodic oscillation for only a few periods. In a longer run the oscillations are not quite periodic, because the borders of the phase domains move, but the oscillations of the average concentration of $Ru(bpy)_3{}^{3+}$ remain periodic. We always obtain C3's when the feedback coefficient is $1.8 < \gamma < 3.1\ s^{-1}$. Within this range the C3's do not overlap with any other pattern, i.e., their formation is independent of the initial conditions. C3's arise also for $0.65 < \gamma < 1.8\ s^{-1}$, but in this case they are not the only pattern found in the system (see Fig. 3). We can observe C3's within this multistable range if we first create a C3 at a higher value of γ, where it is the only stable pattern, and then decrease the feedback coefficient. When γ drops below $0.65\ s^{-1}$, C3's vanish and traveling waves emerge. If we start from a TW pattern and increase the feedback coefficient beyond the TW stability, we usually obtain C2's first; only after $\gamma > 1.8\ s^{-1}$ do the C3's arise. In Fig. 3 this behavior is shown as overlapping of the domains of C2's with part of the TW and part of the C3 domains.

(a) Border movement. As mentioned above, in the case of C2's the borders between domains with different phases become stationary after a transient period. We have not found stationary borders in the case of C3's, even for very long runs. As the domains change phase (and thus the level of $[Ru(bpy)_3{}^{3+}]$) with time, from white to black and then to gray, the border gradually moves in one direction. To follow border movement we take one snapshot per period T and compare borders in these consecutive snapshots. The borders of C3's always drift, following a simple rule: the border moves in the direction that leads to expansion of black domains into white domains, white domains into gray, and gray domains into black. According to this rule, when the domains alternate regularly, their sizes remain almost unchanged and only their positions change with time [Fig. 8(a)]. On the other hand, if a domain is surrounded entirely by domains of a single $[Ru(bpy)_3{}^{3+}]$ level, then there will

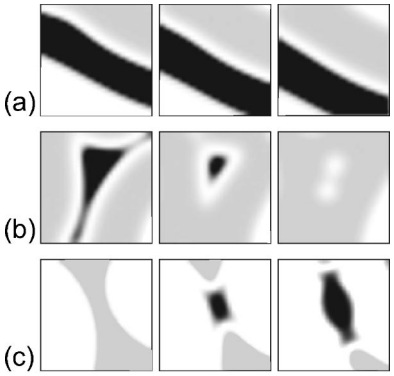

FIG. 8. Border drift and interactions of domains in three-phase clusters. Enlargement of parts of pattern from Fig. 7; displayed area is 1.35×1.35 mm^2. (a) Drift of border domains, snapshots taken at time interval $2T$ apart, where T is period of local oscillations. (b) Annihilation of a domain—snapshots are taken at time intervals T apart. (c) Fusion of two domains of one phase, originally separated by a domain of second phase, results in creation of domain of third phase—snapshots taken at time intervals T apart.

be a size adjustment. Figure 8(b) shows a black domain surrounded by gray domains. The black domain gradually shrinks in size and eventually disappears, as the gray domain engulfs it.

In some cases, we observe another interesting behavior. Figure 8(c) shows a collision between two white domains, which expand through a gray domain. At the point of collision, a small piece of a third (black) domain is created. This new black domain area increases in size with time. The collision thus allows the formation of a ''missing'' third domain at the collision point.

(b) Border curling. Sometimes, three domains with phases shifted by $T/3$ meet at a singular point. Around this point, the borders rotate periodically, creating a cluster spiral wave. This border curling occurs naturally when C3's arise from random initial conditions. One can observe several areas with border curling in Fig. 7. To demonstrate the dynamics of border curling, we employ special initial conditions, which lead to creation of C3's with curling borders. Figure 9 displays such a pattern, which arose from the initial conditions shown in Fig. 9(a). The pattern displays three-phase oscillations on the short time scale, while on the long time scale one can see the movement of domain borders, which

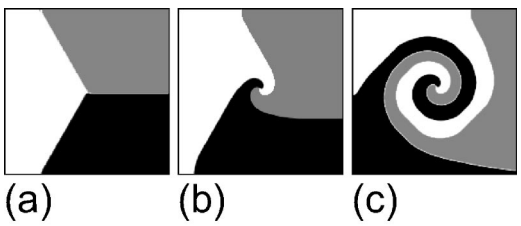

FIG. 9. Three-phase spiral cluster. (a) Initial pattern of three domains with phases shifted by one-third of local period. Point at which three domains meet becomes tip of spiral during long-time border curling movement. (b) Pattern at time $t=48T$. (c) Pattern at time $t=153T$. $\gamma=1$ s^{-1}, local period of oscillations $T=38.16$ s, size of system is 10×10 mm^2.

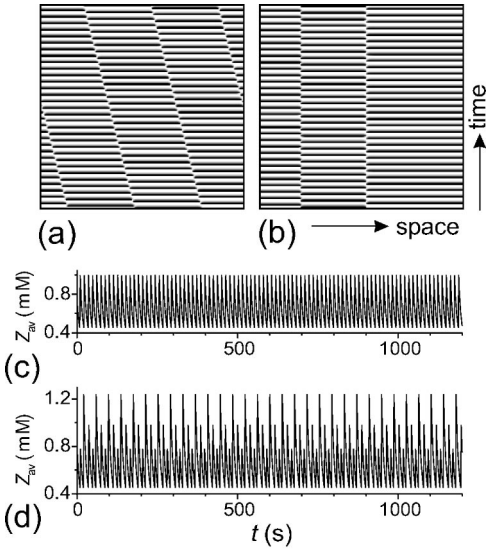

FIG. 10. Three-phase clusters in 1D system. (a) Phase balance is reached in system with periodic boundary conditions. (b) Absence of phase balance in system with zero-flux boundary conditions. (c), (d) Oscillations of average $[Ru(bpy)_3{}^{3+}]$ correspond to patterns shown in (a) and (b), respectively. Length of system is 10 mm. $\gamma=1$ s^{-1}.

form a three-armed spiral. If we take one snapshot per period and display the pattern as a sequence of these snapshots, we see only a rotating three-armed spiral.

(c) Phase balance. We investigate the properties of C3's in both 1D and 2D systems. In a 2D system with either zero-flux or periodic boundary conditions, we find that the sum of the areas belonging to each of three phases always converges to one-third of the total area. Once this phase balance is reached, the oscillations of Z_{av} become periodic with a frequency three times higher than the frequency of the local concentration oscillations. This phenomenon is analogous to the phase balance of C2's, where the frequency of Z_{av} is twice the frequency of the local oscillations. However, in 1D systems phase balance of C3's is not always achieved. The development of phase balance in a 1D system requires periodic boundary conditions, which allow rotational movement of the phase domain borders. After a transient period, which depends on the initial conditions, all borders move at the same constant speed, which indicates that phase balance has been reached [see Figs. 10(a) and 10(b)].

(d) Absence of phase balance. In a 1D system with zero-flux boundaries, movement of domain borders is limited, which results in persistent unequal sizes of the phase domains. The zero-flux boundary conditions do not allow rotational movement of the phase borders, and this prevents the system from reaching phase balance. Movement of the domain borders first leads to a decrease of the area occupied by some of the domains. The border movement eventually stops, and, as Figs. 10(b) and 10(d) show, a stationary pattern is established with unequal areas occupied by domains with different phases. This stable cluster pattern represents an exception to a general rule that oscillatory patterns with period larger than 2 are typically metastable rather than stable [21,22].

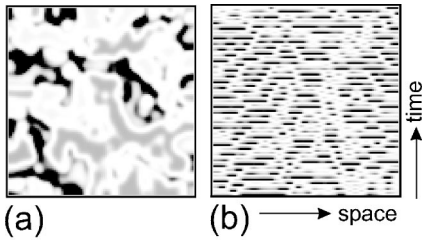

FIG. 11. Irregular cluster pattern in 2D system with zero-flux boundary conditions. (a) Snapshot of pattern. (b) Corresponding spatiotemporal behavior along horizontal line at midpoint of vertical axis. Time shown is 1290 s. $\gamma = 3.2\ s^{-1}$; size of system is $5 \times 5\ mm^2$.

3. Irregular Clusters

At relatively large γ ($>3.1\ s^{-1}$), another type of pattern arises. In this case, local oscillations in domains of different phases are not periodic, even during a short period of time, as in the case of C3's, and we dub these patterns irregular clusters. Figure 11 shows a pattern of IC's. Any type of initial conditions results in a random distribution of black, gray, and white domains, as shown in Fig. 11(a), and an absence of stationary node lines, shown in Fig. 11(b). Figure 12 shows oscillations at one arbitrarily chosen point together with oscillations in the average concentration Z_{av}. Figure 12 demonstrates that local oscillations of IC's are aperiodic, while the global oscillations are nearly periodic.

4. Localized clusters

The IC's shown in Fig. 11 display irregular oscillations at every point of the system [see Fig. 11(b)]. When the system is inside the oscillatory region, far from the Hopf bifurcation lines (point P in Fig. 1), this pattern gives way to small-amplitude bulk oscillations when $\gamma > 3.5\ s^{-1}$. When parameters B and h_0 are close to the Hopf bifurcation line separating the oscillatory region from the reduced steady state region, we do not obtain C3's, but instead patterns of localized clusters (LC's) arise. Figures 13(a) and 13(b) show localized irregular clusters. In this case IC's occupy only a part

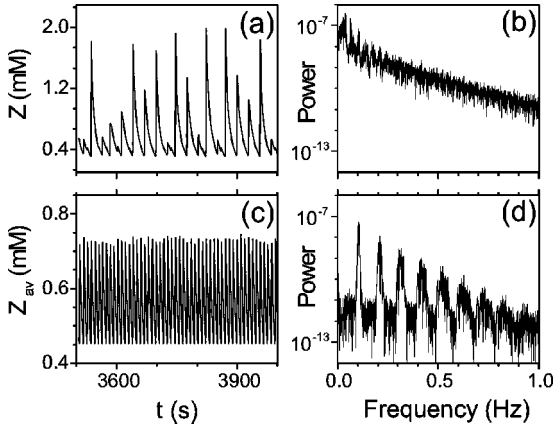

FIG. 12. Local and global oscillations of irregular cluster pattern shown in Fig. 11. (a) Oscillations at a point and (b) corresponding power spectrum. (c) Oscillations of average concentration of $Ru(bpy)_3^{3+}$ and (d) corresponding power spectrum. Main peak is located at frequency 0.104 Hz.

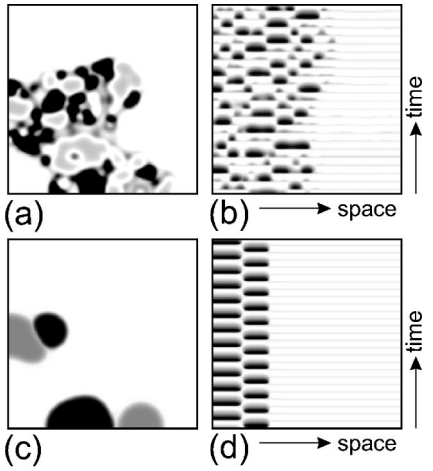

FIG. 13. Irregular and regular localized clusters in vicinity of Hopf bifurcation (near reduced steady state). (a) Snapshot of localized irregular cluster and (b) corresponding spatiotemporal pattern, $\gamma = 0.5\ s^{-1}$. (c) Snapshot of regular localized standing cluster and (d) corresponding spatiotemporal pattern, $\gamma = 0.7\ s^{-1}$. Spatiotemporal patterns are taken along horizontal line at midpoint of vertical axis. Time shown in (b) and (d) is 1080 s. Parameters: $h_0 = 0.19$ M, $B = 0.27$ M. Size of system is $10 \times 10\ mm^2$.

of the space, while in the remaining part small-amplitude bulk oscillations occur. When γ is increased further, the area of SBO's increases. Then, a pattern of localized C2 clusters emerges [Figs. 13(c,d)], which displays regular periodic oscillations in domains that occupy a small part of the space. This pattern, which has stationary nodal lines, has been described in Ref. [16]. Finally, when $\gamma > 3.5\ s^{-1}$, the system displays uniform small-amplitude bulk oscillations.

When the parameters are close to the boundary with the oxidized steady state, we obtain only C2's at intermediate values of the feedback coefficient. Both weak and strong feedback result in uniform oscillation, but with large and small amplitude, respectively.

IV. DISCUSSION AND CONCLUSION

We have studied pattern formation in a realistic model of the photosensitive BZ reaction. A plethora of reaction-diffusion patterns arise when the feedback coefficient is varied. We focus here on cluster formation. At relatively low values of the feedback coefficient, two- and three-phase clusters arise, each of which consists of uniform domains. Inside the domains, oscillations are synchronous. The domains form patterns which usually lack spatial periodicity, since global feedback does not produce a characteristic wavelength. During the evolution of these patterns, global feedback plays an important role in establishing equality between the areas occupied by domains of different phases. Border curling of three-phase clusters may lead to formation of spiral clusters—a fast oscillating cluster with a slow three-arm spiraling movement of the borders. At higher feedback coefficient, irregular cluster patterns arise. Local oscillations of irregular clusters are aperiodic in time; however, oscillations of the average $[Ru(bpy)_3^{3+}]$ remain periodic in this case. Localized clusters arise only for parameters near the Hopf line, and they display regular or irregular clusters, which

occupy only a part of the space, while the remaining part displays small-amplitude bulk oscillations.

We are not aware of other work demonstrating three-phase clusters as a result of global feedback coupling. Moreover, the C3's obtained in the BZ model with global feedback are found in a relatively wide parameter region with no other overlapping pattern. This means that three-phase clusters arise from any initial conditions. The existence of C3's in the BZ reaction with global feedback has been confirmed experimentally in our laboratory [23]. Unlike standing waves, clusters do not possess an intrinsic wavelength and thus they can maintain a pattern of initial conditions indefinitely. This suggests the possibility of creating a system with pattern memory. If one illuminates a layer of photosensitive BZ reaction mixture through a mask imprinted with an image and then applies global feedback, the initial image can be maintained in the form of C2's for some time. Such an experiment may be thought of as an extension of the study by Kuhnert *et al.* [24], in which the authors succeeded in transiently preserving photographic images in ruthenium-catalyzed BZ reaction mixtures.

ACKNOWLEDGMENTS

We gratefully acknowledge the support of the National Science Foundation Chemistry Division and the W. M. Keck Foundation. We thank Vladimir Vanag for helpful comments and discussions.

[1] A.N. Zaikin and A.M. Zhabotinsky, Nature (London) **225**, 535 (1970).
[2] A.T. Winfree, Science **175**, 634 (1972).
[3] *Chemical Waves and Patterns*, edited by R. Kapral and K. Showalter (Kluwer, Dordrecht, 1995).
[4] D. Golomb, D. Hansel, B. Shraiman, and H. Sompolinsky, Phys. Rev. A **45**, 3516 (1992).
[5] V. Hakim and W.-J. Rappel, Phys. Rev. A **46**, 7347 (1992).
[6] M. Falcke and H. Engel, J. Chem. Phys. **101**, 6255 (1994).
[7] M. Falcke, H. Engel, and M. Neufeld, Phys. Rev. E **52**, 763 (1995).
[8] M. Bär, M. Hilderbrand, M. Eiswirth, M. Falcke, H. Engel, and M. Neufeld, Chaos **4**, 499 (1994).
[9] O. Lev, M. Sheintuch, L.M. Pisemen, and Ch. Yarnitzky, Nature (London) **336**, 458 (1988).
[10] S. Jakubith, H.H. Rotermund, W. Engel, A. von Oertzen, and G. Ertl, Phys. Rev. Lett. **65**, 3013 (1990).
[11] M. Somani, M.A. Liauw, and D. Luss, Chem. Eng. Sci. **52**, 2331 (1997).
[12] G.A. Cordonier, F. Schuth, and L.D. Schmidt, J. Chem. Phys. **91**, 5374 (1989).
[13] A.M. Zhabotinsky, M. Dolnik, and I.R. Epstein, J. Chem. Phys. **103**, 10 306 (1995).
[14] M. Dolnik, A.B. Rovinsky, A.M. Zhabotinsky, and I.R. Epstein, J. Phys. Chem. **103**, 38 (1999).
[15] M. Dolnik, A.M. Zhabotinsky, A.B. Rovinsky, and I.R. Epstein, Chem. Eng. Sci. **55**, 223 (2000).
[16] V. Petrov, Q. Ouyang, and H.L. Swinney, Nature (London) **388**, 655 (1997).
[17] V.K. Vanag, L. Yang, M. Dolnik, A.M. Zhabotinsky, and I.R. Epstein, Nature (London) **406**, 389 (2000).
[18] S. Kadar, T. Amemiya, and K. Showalter, J. Phys. Chem. A **101**, 8200 (1997).
[19] A.M. Zhabotinsky, F. Buchholtz, A.B. Kiyatkin, and I.R. Epstein, J. Phys. Chem. **97**, 7578 (1993).
[20] A. Bugrim, M. Dolnik, A.M. Zhabotinsky, and I.R. Epstein, J. Phys. Chem. **100**, 19 017 (1996).
[21] C.H. Bennett, G. Grinstein, Y. He, C. Jayaprakash, and D. Mukamel, Phys. Rev. A **41**, 1932 (1990).
[22] P.-M. Binder and J.F. Jaramillo, Phys. Rev. E **56**, 2276 (1997).
[23] V. Vanag, A.M. Zhabotinsky, and I.R. Epstein (unpublished).
[24] L. Kuhnert, K.I. Agladze, and V.I. Krinsky, Nature (London) **337**, 244 (1989).